High Performance Capacitors Using $BaTiO_3$ Nanostructures Engineered Rigid Liquid-crystalline Polymers

Abstract: Capacitors that provide high power density have attracted scientific and commercial interest, while often suffering from low energy density. Preparing a core–shell structured ceramic is regarded as a kind of effective method to improve the energy density, which is largely determined by the shell in the interfacial region. However, the current state-of-the-art of interfacial layer modification is predominantly based on utilizing flexible polymers, which are random polymer coils that collapse on the surface of any modified ceramic nanoparticles. Because of the characteristic properties of rigidity and orientation, the liquid-crystalline polymer poly{2,5-bis[(4-methoxyphenyl)oxycarbonyl]styrene} (PMPCS) is utilized to engineer the interfacial layer thickness on $BaTiO_3$ nanowire surfaces via surface-initiated reversible addition–fragmentation chain transfer polymerization (RAFT) method, in this paper. As a result, a high discharged energy density of 7.5 J/cm^3 and an energy efficiency of 55.1% at 300 MV/m are achieved, respectively. The findings proved that rigid liquid-crystalline polymer is a promising modifier to prepare high performance capacitors and to explore the interfacial effect in dielectric nanocomposites.

Key words: liquid-crystalline polymers; discharged energy density ; $BaTiO_3$ Nanostructures**,** interfacial region; core-shell structure

1. Introduction

By 2020, the European Union (EU) aims to reduce greenhouse gas emissions by 20-30% and increase the renewable energy share to 20%.[1] This scenario has imposed an urgent need to develop alternatives to fossil fuel, such as solar fuels. Compared to solar fuels, lithium batteries and other renewable energy systems, capacitors possess a superior power density, and are therefore widely applied in electronic devices with pulsed power such as radar, electric vehicles, mobile electronics, lasers, and rail guns.[2-8] However, high power capacitors usually suffer from a low energy density, making them both bulky and expensive. To achieve high energy density, dielectric materials with high relative permittivity, high breakdown strength and low dielectric loss are required.[9] At present, significant attention is focused on the development of ceramic/polymer nanocomposites to combine the high permittivity of ferroelectric ceramic fillers with the high dielectric strength and facile processability of a polymer.[10] For example, in our previous work, high loading levels of $BaTiO_3$ and $Pb(Mg_{1/3}Nb_{2/3})O_3$–$PbTiO_3$ (PMN-PT) spherical particles were incorporated into a ferroelectric polymer poly(vinylidene fluoride-hexafluoropropylene) (P(VDF-HFP)). This enabled a significantly higher permittivity than P(VDF-HFP) to be achieved, but at the expense of a decreased breakdown strength compared to the pure polymer

matrix phase.[11, 12]

Despite the promising potential of the ceramic/polymer hybrid systems, the large difference of surface energies between ceramic fillers and its polymer matrix phase inevitably lead to nanoparticle aggregation, cracks and voids in the polymer matrix, particularly in the case of high nanoparticle loading levels.[13] In addition, the high contrast of permittivity between the two phases can create distortion and inhomogeneity of the electric field distribution throughout the composite microstructure. These problems are harmful to the electrical properties of the nanocomposites, for example the field concentrations can lead to an increase of dielectric loss and a decrease of breakdown strength.[14] Therefore, approaches to balance and tailor the permittivity and breakdown strength needs to be investigated. One approach is to control of shape, size, and orientation of the ceramic fillers relative to the applied electric field. Recently, one-dimensional fillers has been proven to be a superior choice to obtain composite systems with a high energy storage density due to the more effective increase of permittivity, breakdown strength and lower percolation threshold compared to spherical particle/polymer systems.[15-17] Another approach is surface modification of ceramic fillers. Ceramic fillers in dielectric composites generally possess a nano-scaled size and as a result the interface area between the ceramic filler particles and the polymer matrix plays a dominant role in the nanocomposites. The interface can be tailored through surface modification by specific organic small molecules, such as phosphonic acid[18] and ethylene diamine,[10] which can decrease the surface energy of the nano-filler and bridge the gap between

the nano-filler and the polymer matrix.[19, 20] However, any unabsorbed residual molecules can lead to a high leakage current and dielectric loss due to the weak interaction.[21] Recently, a more effective strategy is to employ a surface-initiated reversible addition−fragmentation chain transfer polymerization (RAFT) or in situ atom transfer radical polymerization (ATRP); these approaches are used to control the interface by grafting polymers with a well-defined molecular weight and tailor electrical properties on the nano-filler surface, resulting in improved nano-filler dispersion in the polymer matrix and improved electrical properties of the polymer nanocomposites.[20, 22, 23] It is worth noting that the applied modifiers are predominantly flexible organic molecules and polymers, which consists of random coils that simply collapse on the surface of the modified ceramic fillers. As a result, the thickness and morphology of the modified layer cannot be finely tuned.[24] Most reports to date indicate that the organic coated layer thickness is limited to 2~6 nm, which cannot fully encapsulate the bare nano-fillers due to the filler roughness.[11, 14, 25]

Mesogen-jacketed liquid crystalline polymers (MJLCPs) proposed by Zhou et al. in 1987 have attracted increasing interest for its novel structures and intriguing properties, such as high glass transition temperature, broad temperature range of mesophase, the formation of a banded texture after mechanical shearing in the liquid-crystal (LC) state and the ability to be an ideal rod-forming system.[26-30] Crowded, rigid, and bulky side groups have been attached laterally to the main chain through a short spacer or with a single covalent bond in MJLCPs. Poly{2,5-bis[(4-methoxyphenyl)oxycarbonyl]styrenes} (PMPCS) is a typical

rigid-polymer in MJLCPs family.[31] Due to the strong spatial effects on the main chain by rigid and bulky side groups, the polymers take an extended and stiffened conformation and order into a columnar phase, as in main-chain, when the molecular weight of PMPCS is beyond 1.0×10^4. The size of the straight conformation unit can be calculated by Eqn. 1:[32]

$$L_{rod} = 0.154(nm)\times 2N_{rod}\times \sin 52^o \approx 0.24N_{rod}(nm), \qquad (1)$$

where L_{rod} and N_{rod} are size of the columnar phase unit and polymerization degree of PMPCS, respectively.

To enhance the surface area of the ceramic filler, one dimensional 'bamboo-like' $BaTiO_3$ nanostructures were synthesized by hydrothermal method in this work. A PMPCS rigid-polymer was used to engineer for the first time the surface of the $BaTiO_3$ nanostructures via a surface-initiated RAFT. Interestingly, the thickness of the polymer shell layer could be finely tailored by utilizing the characteristic feature of rigidity and the orientation and controlling the molecular weight of PMPCS according to Eqn. 1. Due to the growth of a thick PMPCS coating layer on the $BaTiO_3$ nanostructures, ~33 nm thick, the nanocomposite exhibited a high discharged energy density and energy efficiency. This work therefore provides an effective strategy to finely tune the interfacial layer thickness and prepare dielectric nanocomposites with high discharged energy density based on the rigid liquid-crystalline polymers.

2. Experimental section

2.1 Materials

P(VDF-HFP) pellets with less than 15 wt% of HFP was purchased from Aldrich. An

aqueous solution of H_2O_2 (30 wt %), N, N-dimethylformamide (DMF), dichloromethane (DCM), and other organic reagents or solvents was supplied by Shanghai Reagents Co. Ltd. N-hydroxysuccinimide (NHS), N,N'-dicyclohexylcarbodiimide (DCC), 4-dimethylaminopyridine (DMAP), and γ-aminopropyl triethoxysilane (γ-APS) were purchased from Acros. 2,2'-azobis (2-methylpropionitrile) (AIBN, 99%, Aldrich) were used in 'as received' condition. All other chemicals were used 'as received', except for those noted.

2.2 Synthesis of 'bamboo-like' $BaTiO_3$ nanostructures

The high surface area bamboo-like $BaTiO_3$ nanostructures (b-BT NS) were synthesized by hydrothermal method. Firstly, 1.446 g titanium oxide (TiO_2, anatase) was added to 70 ml NaOH solution (10 M) and the mixture was stirred for 2 h to form a homogeneous suspension. The hydrothermal reactions were carried out at 210 °C under auto-generated pressure for 24 h in a 100 ml Teflon-lined autoclave. The products were washed using distilled water and then soaked in diluted 0.2 M hydrochloric acid (HCl, 37%) for 4 hours to obtain hydrogen titanate nanofibers ($H_2Ti_3O_7$ NFs). Secondly, 0.150 g $H_2Ti_3O_7$ were dispersed in 70 ml $Ba(OH)_2{\cdot}8H_2O$ solution and the mixture was sonicated for 10 min. The hydrothermal reactions were carried out at 210 °C under auto-generated pressure for 24 h in a 100 ml Teflon-lined autoclave. The products were soaked in 0.2 M HCl solution briefly, then washed by distilled water several times and dried at 80 °C in oven.

2.3 Synthesis of monomer MPCS

The detailed synthetic procedure and the chemical characterization of the monomer

were reported.[33] The synthetic procedure is illustrated in scheme 1. The characterization data of monomer was as follows: ^{1}H NMR, (400 MHz, δ, $CDCl_3$): 8.16-8.42 (m, 3H of phenyl), 7.49-7.52 (q, 1H of –CH=), 6.93-7.16 (m, 8H of phenyl), 5.41-5.85 (2 d, 2H of dCH_2), 3.82 and 3.85 (2 s, 6H of -OCH_3).

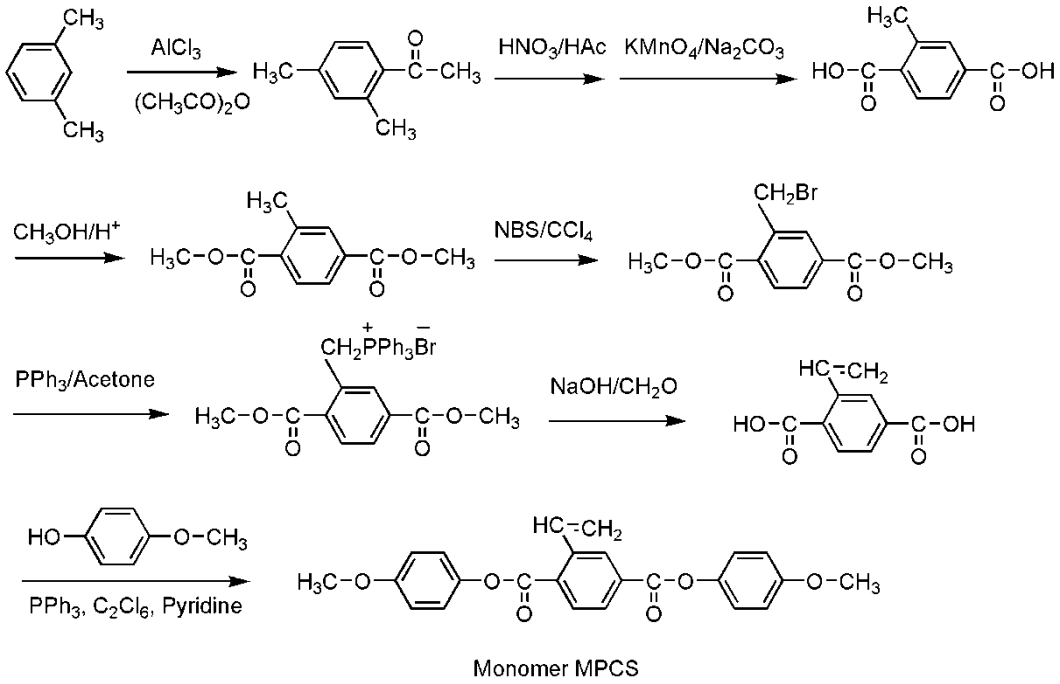

Scheme 1. Synthetic route of 2,5-bis[(4-methoxyphenyl)oxycarbonyl]styrenes (MPCS) monomer

2.4 Preparation of RAFT agent CPDB-anchored $BaTiO_3$ nanostructures

2.4.1 Synthesis of 4-cyanopentanoic acid dithiobenzoate (CPDB)

The synthetic procedure is shown in scheme 2 and a detailed synthesis route is given in the following description. A dry 0.5 L three-necked round-bottomed flask equipped with a magnetic stir bar, addition funnel (250.0 mL) and rubber septum for liquid transfer was filled with THF and CS_2 and then Mg (1.31g, 55mmol), a small amount of I_2, and 90ml THF were added. Bromobenzene (7.79 g, 50 mmol) and 25 ml THF were then added dropwise via the addition funnel over a period of 1 h at 50^{o}C

under a dry nitrogen atmosphere. The reaction mixture was heated in an oil bath at 50 °C for 5h. After this time, the reaction mixture was cooled to room temperature. Then, 30ml (4.5 g, 60 mmol) CS_2 and 30ml THF were added to the flask via a cannula. The reaction mixture was then heated in an oil bath at 50 °C for 3h.

The solvent mixture was removed in vacuum leaving a red oily residue which was added into a 250ml K_2CO_3 solution (10 wt%). The precipitated salt ($MgSO_4$) was removed by filtration and the aqueous solution was washed by diethyl ether. The 60 ml 1.2N I_2/KI solution was added into the aqueous solution while stirring. The mixture solution was extracted with CH_2Cl_2. The solvent was then removed in vacuum and finally the target compound (4-cyanopentanoic acid dithiobenzoate, CPDB) was obtained.

2.4.3 Activation of CPDB

CPDB (1g), 2-mercaptothiazoline (0.45 g), and dicyclohexylcarbodiimide (DCC) (0.81 g) were dissolved in 20 mL of dichloromethane. (Dimethylamino) pyridine (DMAP) (40mg) was added slowly to the solution and the mixture was stirred at room temperature for 10 h. The solution was filtered to remove the salt. After removal of the solvent and a silica gel column chromatography (5:4 mixture of hexane and ethyl acetate), the activated CPDB was obtained as a red oil (0.5 g, 50% yield). ^{1}H NMR, (400 MHz, δ, $CDCl_3$): 7.90 (d, 2H, aromatic ring), 7.56 (t, 1H, aromatic ring), 7.39 (t, 2H, aromatic ring), 4.58 (t, 2H, NC**H**$_2$CH$_2$S), 3.70-3.62 (m, 2H, (CN)C(CH$_3$)-CH$_2$**C**H$_2$CON), 3.31 (t, 2H, NCH$_2$*C***H**$_2$S), 2.55-2.62 (m, 2H, (CN)C(CH$_3$)**C**H$_2$CH$_2$CON), 1.95 (s, 3H, (*C***H**$_3$)C(CN)S).

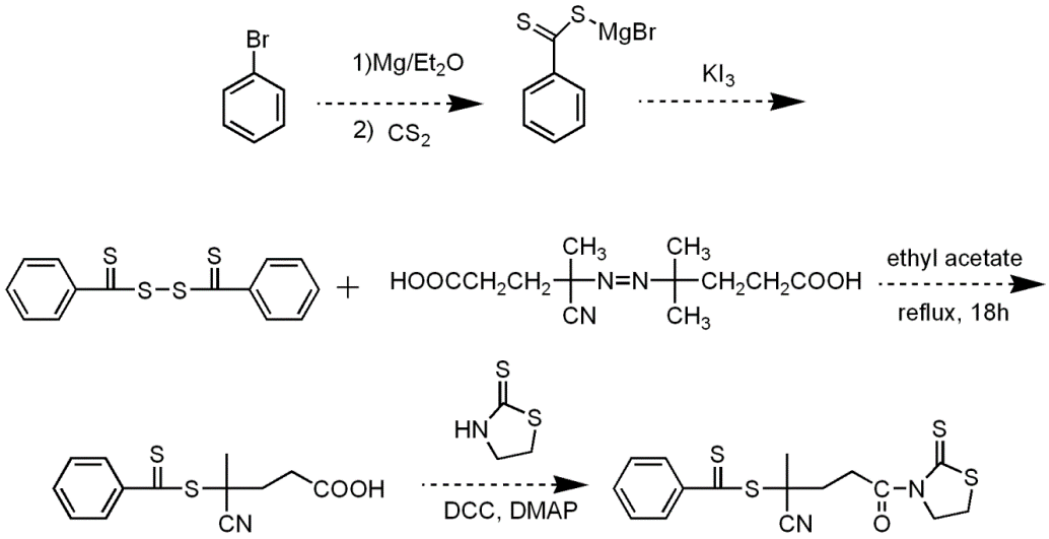

Scheme 2. Synthetic route of activation of the RAFT agent 4-cyanopentanoic acid dithiobenzoate (CPDB-NHS)

2.4.4 Preparation of amino-functionalized $BaTiO_3$ nanostructures

A mass of 4 g of b-BT NS was added to a three-necked round-bottom flask with 3-aminopropyldimethylethoxysilane (2.0 g, 1.2 mmol) and dried THF (25 mL). The reaction mixture was heated at 85 °C under N_2 protection overnight and then cooled to room temperature. The nanofibers were recovered by centrifugation at 8000 rpm for 5 min and washed with THF three times. The obtained aminofunctionalized $BaTiO_3$ ($BaTiO_3$−NH_2) nanostructures were then dried under vacuum at 80 °C for 24 h.

2.4.4 Preparation of CPDB-anchored $BaTiO_3$ nanostructures

$BaTiO_3$−NH_2 (4 g) was dispersed in THF and sonicated for 30 min. The mixture was then added dropwise to a THF solution of CPDB-NHS (0.60g) at 0 °C with vigorous stirring. The reaction mixture was kept at 0 °C for 6 h, allowed to gradually warm to room temperature, and then left to stir for 12 h. The $BaTiO_3$−CPDB obtained by centrifugation at 8000 rpm for 5 min and washed with THF three times were then

dried under vacuum at 60 °C for 24 h.

2.5 Surface-initiated RAFT polymerization of PMPCS on b-BT NS

The typical procedure was carried out as follows: 0.4g MPCS, 84 μL of chlorobenzene solution of 0.01 g/ml AIBN, 2.7g of chlorobenzene, 0.4g $BaTiO_3$−CPDB and a magnetic stir bar were added into a polymerization tube. After three freeze-pump-thaw cycles, the tube was sealed off under vacuum. Polymerization was carried out at 70 ^{o}C for 6 h. The tube was then opened, and the reaction mixture was diluted with 8 mL of THF and centrifuged to decant the supernatant. The pristine PMPCS@$BaTiO_3$ nanostructure was then washed with THF four times. The product was dried under vacuum at 80 °C for 24 h.

2.6 General procedures for cleaving grafted polymer from b-BT NS

In a typical experiment, 50 mg of PMPCS grafted $BaTiO_3$ nanostructures were dissolved in 3 mL of THF. Aqueous HF (49%, 0.2 mL) was added, and the solution was allowed to stir at room temperature overnight. The solution evaporated in a fume hood for several days. The recovered PMPCS was then subjected to GPC analyses.

2.7 Fabrication of P(VDF-HFP) nanocomposite films

$BaTiO_3$**@**PMPCS nanostructures were dispersed in *N*, *N*-dimethylformamide (DMF) (Guoyao from China) firstly, and mixed with P(VDF-HFP) with ultrasound and stirring for further dispersion. The resultant suspension was then cast onto clean glass, and dried at 80 °C for 12 h under vacuum. The dried nanocomposite sheets were compressed into films at 200 °C under a pressure of approximately 15 MPa. The thickness of the final composite film was 10~20 μm. Gold electrodes were sputtered

on both sides of the film using a mask with 2 mm diameter eyelets.

2.8 Characterization

The crystalline phases of the $Na_2Ti_3O_7$ and b-BT NS were evaluated by X-ray diffraction (XRD, D/max 2550, Japan) with Cu-Kα radiation (λ=1.5406 Å) at room temperature. The size and morphology of the $BaTiO_3$ and nanocomposite films were examined using a scanning electron microscope (SEM, Nova NanoSEM230, USA). High-resolution transmission electron microscopy (HRTEM) images of the b-BT NS were taken with a Titan G2 60-300, using an accelerating voltage of 300 kV. The frequency-dependent dielectric constant and dielectric loss of the nanocomposite films were measured using an Agilent 4294A LCR meter with frequency ranging from 100 Hz to 10 MHz. ^{1}H NMR spectroscopy was performed on a Bruker ARX400 MHz spectrometer using with $CDCl_3$ as solvent, tetramethylsilane (TMS) as the internal standard at ambient temperature. The chemical shifts were reported on the ppm scale. The apparent number average molecular weight (M_n) and polydispersity index (PDI = M_w/M_n) were measured on a GPC (WATERS 1515) instrument with a set of HT3, HT4 and HT5. The μ-styragel columns used THF as an eluent and the flow rate was 1.0 ml/min at 30 ^oC. All GPC data was calibrated with polystyrene standards. The liquid crystal texture of the polymers was examined under polarised optical microscopy (Leica DM-LM-P) equipped with a Mettler Toledo hot stage (FP82HT). One-dimensional wide-angle X-ray diffraction (1D WAXD) experiments were performed on a BRUKER AXS D8 Advance diffractometer with a 40 kV FL tubes as the X-ray source (Cu Kα) and the LYNXEYE-XE detector. Background

scattering was recorded and subtracted from the sample patterns. The heating and cooling rates in the 1D WAXD experiments were 10 ^{o}C/min. The polarization-electric field (P-E loops) of the nanocomposite were measured at 10 Hz at room temperature by a TF analyzer 2000 ferroelectric polarization tester (aixACT, Germany) and Delta 9023 furnace in a silicone oil bath to avoid any electrical discharges that would occur in air.

Results and Discussion

Preparation and Characterization of $BaTiO_3$@PMPCS Nanostructures

Figure 1a, 1b and 1c show the morphology of hydrothermally synthesized $Na_2Ti_3O_7$ nanofibers, $H_2Ti_3O_7$ nanofibers and b-BT NS. The $Na_2Ti_3O_7$ nanofibers possessed a high aspect ratio and smooth surface. The b-BT NS synthesized by a second hydrothermal reaction had an average diameter of approximately 200 nm and length of approximately 2.5 μm. As can be seen, the morphology of synthesized $BaTiO_3$ is different to the $Na_2Ti_3O_7$ and $H_2Ti_3O_7$ nanofibers, which exhibited a number of small knots on the surface, while the morphology of $BaTiO_3$ was similar to bamboo, defined as bamboo-like $BaTiO_3$ nanostructures (b-BT NS) in the remainder of this paper. Figure 1d shows XRD pattern of $Na_2Ti_3O_7$ nanofibers and b-BT NS, which can be indexed to monoclinic $Na_2Ti_3O_7$ (PDF card NO. 31-1329) and tetragonal $BaTiO_3$ (PDF card NO. 75-0462) without any impurity phase.

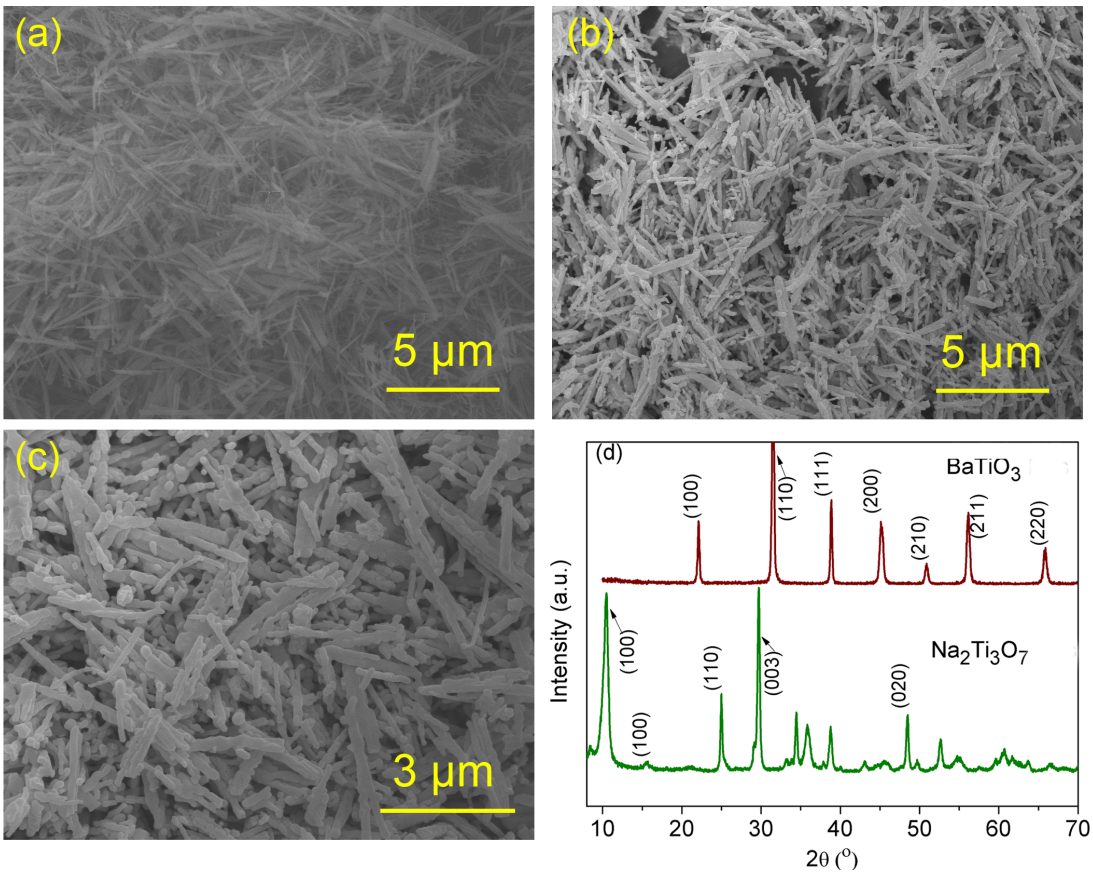

Figure 1 SEM images of (a) $Na_2Ti_3O_7$ nanofibers, (b) $H_2Ti_3O_7$ nanofibers, (c) $BaTiO_3$ nanostructures (b-BT NS), and (d) XRD pattern of $Na_2Ti_3O_7$ and b-BT NS.

Figure 2a and 2b show the bright field TEM images of b-BT NS at low and high magnifications, respectively. It is clear that the morphology of the b-BT NS was rough and bamboo-like. In addition, Figure 2c and 2d show the HR-TEM image and corresponding SAED pattern of a typical b-BT NS, indicating the formation of single-crystalline material. The HR-TEM image shows clear lattice fringes and the parallel lattice spacing were approximately 0.406 nm and 0.286 nm, corresponding to (001) and (101) planes of the tetragonal $BaTiO_3$ phase respectively. This indicates that the b-BT NS grew in the [001] direction.

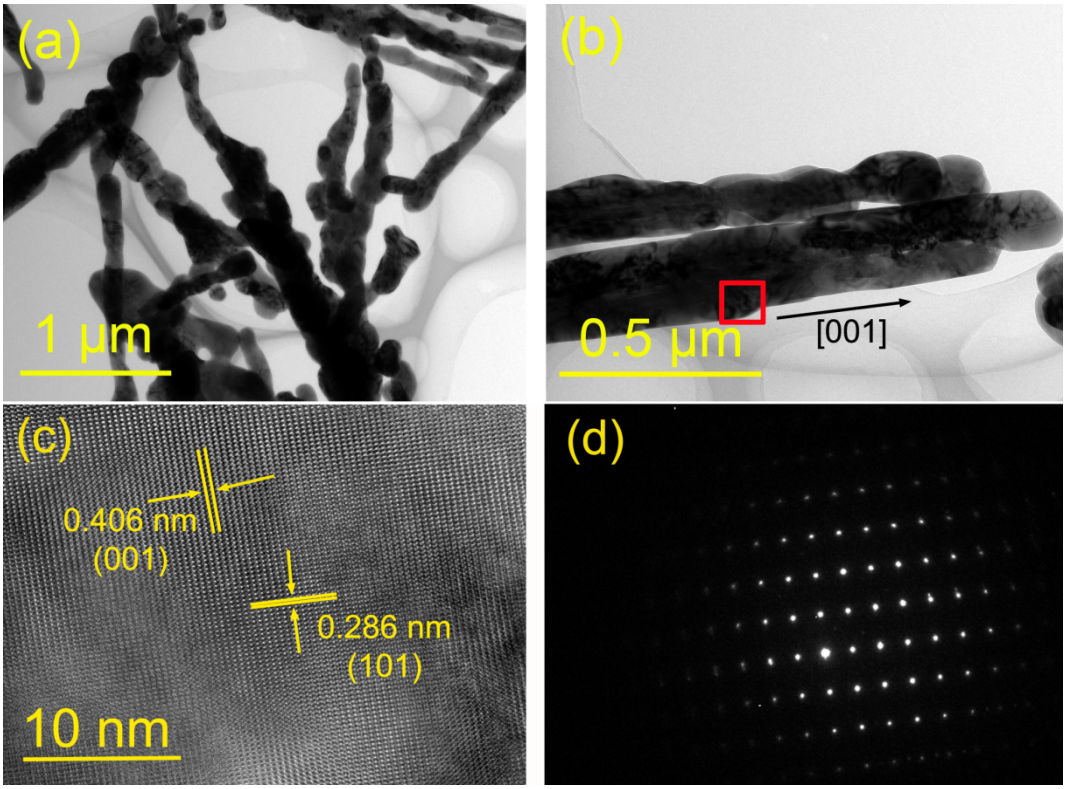

Figure 2 Bright field TEM images of $BaTiO_3$ nanostructures in (a) low and (b) high magnification, (c) HRTEM image and (d) SAED pattern of b-BT NS.

Figure 3 shows the preparation process and structure of the $BaTiO_3$@PMPCS nanostructures. A 'mace-like' structure is obtained, which consists of nanoscale sticks from the b-BT NS (purple regions in Schematic 1a) and spikes that originate from the rigid PMPCS column units (green regions in Schematic 1a). The size of mace-like structure is determined by the length and diameter of the original b-BT NS, and the length of PMPCS column units. The PMPCS column units were designed to be grafted onto the surfaces of b-BT NS via in situ RAFT polymerization. To achieve this, the RAFT agent (CPDB) had to be grafted onto the b-BT NS surface. However, aminolysis of the thioester groups of CPDB agent would occur via reaction with amino groups from the silanes grafted onto the nanoparticle surface. Therefore, the

CPDB was first activated by NHS to keep the thioester groups of the RAFT agent from aminolysis. ^{1}H NMR spectra were used to prove the successful formation of CPDB-NHS (see Figure S1 in Supporting Information). After the CPDB-NHS was grafted onto the nanoparticle surface, the well-defined rigid-polymers PMPCS with designed molecular weights and narrow polydispersities could be readily synthesized by RAFT at the b-BT NS surface at 70 ^{o}C in chlorobenzene using AIBN as the initiators and CPDB-anchored b-BT NS as the chain transfer agent.

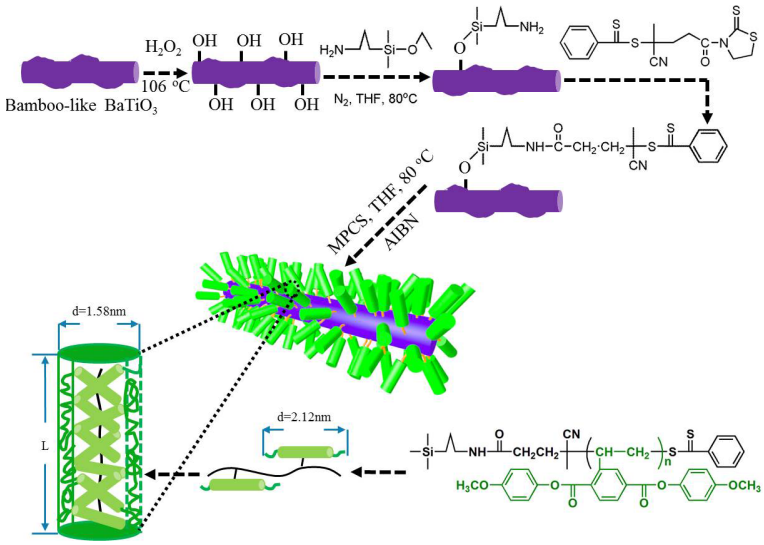

Figure 3 Preparation process and formation of 'mace-like' structure of $BaTiO_3$@PMPCS

Figure 4a-b shows the ^{1}H NMR spectra of pure PMPCS and $BaTiO_3$@PMPCS nanostructures. All the proton signals of PMPCS graft polymerization were found in ^{1}H NMR spectra of pure PMPCS. Surface grafting of the rigid-polymers on the surface of the b-BT NS was further verified by FT-IR spectra. Compared with the FT-IR spectrum of as-prepared b-BT NS, see Figure 4(c), the FT-IR spectrum of $BaTiO_3$@PMPCS exhibit new absorption bands at 1505 and 1736 cm^{-1}, which are

attributed to the phenyl ring stretching vibrations and the carbonyl stretching vibration, respectively. Thermogravimetry (TGA) was also used to prove the successful completion of the surface modification of the b-BT NS. As can be seen from Figure 4d, the $BaTiO_3$@PMPCS show a higher weight loss (15.6%) compared to b-BT NS with the small molecular modifier (2-3%). Finally, digital images showed that the suspensions of the $BaTiO_3$@PMPCS nanostructures in THF remain stable for 2 h after ultrasonic mixing (see Figure S2 in Supporting Information). In summary, based on the ^{1}H NMR, FT-IR spectrum, TGA and the dispersion stability experiment the $BaTiO_3$@PMPCS nanostructures was successfully synthesized and exhibit excellent dispersibility.

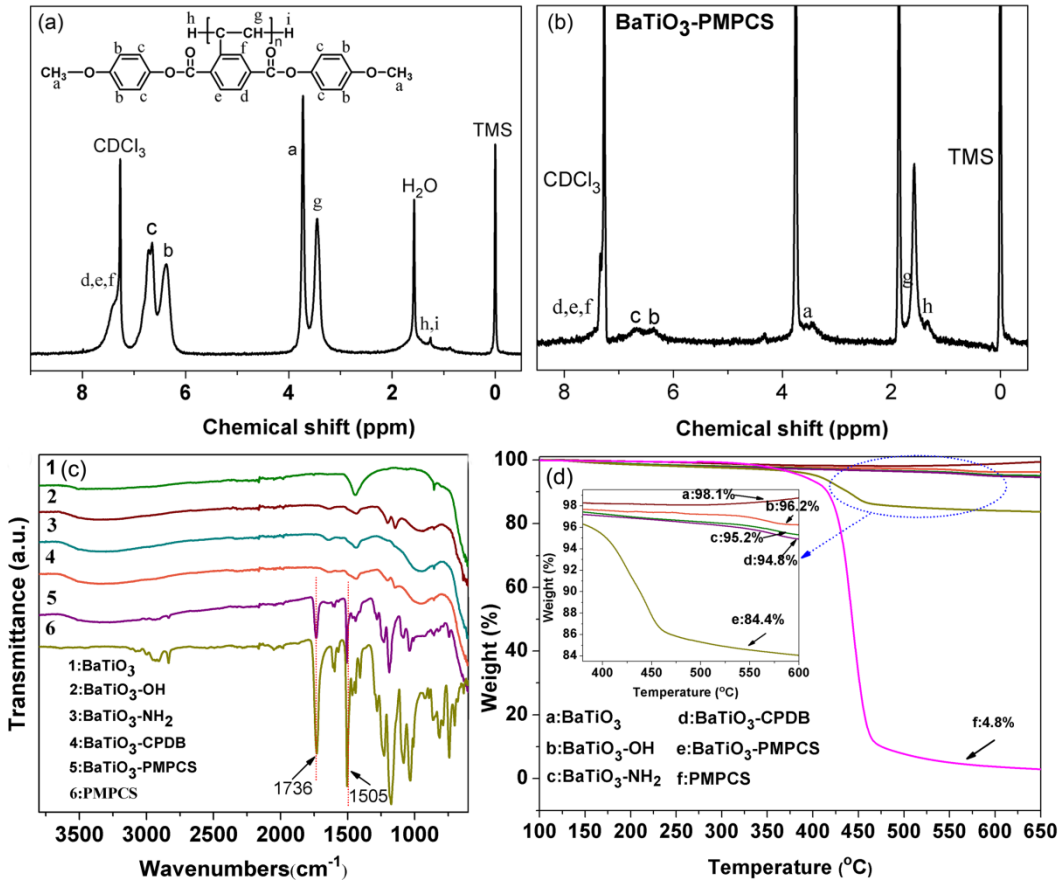

Figure 4 ^{1}H NMR spectra of (a) pure PMPCS and (b) $BaTiO_3$@PMPCS in $CDCl_3$; (c)

FT-IR spectra and (d) TGA cures of $BaTiO_3$ and functionalized $BaTiO_3$ structures.

In order to determine the molecular weight of the grafted PMPCS polymers, cleaving of the grafted polymer from the b-BT NS was performed and gel permeation chromatography (GPC) performed, where the trace is in Figure S2 (Supporting Information). The number-average molecular weight (Mn) of the grafted polymers PMPCS was 6.5×10^4, and the polydispersity index (PDI) and average degree of polymerization (DP) was 1.6 and 100 respectively. Although it is known that the PMPCS is a rigid-polymer when the weight molecular is above 1.0×10^4, the phase structure of grafted polymers PMPCS was investigated by polarized optical microscopy (POM) to observe birefringence of the polymers and 1D/2D WAXD. The sample was cast from THF solution and slowly dried at room temperature. The result showed the grafted polymers exhibited strong birefringence, implying the polymers formed a liquid crystalline phase. From the 1D WAXD pattern (see Figure 5(b)), a strong diffraction peak was detected at 5.7º (with a d spacing of 1.55 nm) at low angle and an amorphous halo around 20º could be observed, indicating that ordered structures on the nanometer scale had formed. Figure 5 c and d present the 2D WAXD patterns at room temperature of the oriented of grafted polymers PMPCS with the X-ray incident beam perpendicular and parallel to the fiber axis, respectively. A pair of strong diffraction arcs can be seen at 5.8° (d spacing of 1.52 nm), indicating that ordered structures have developed along the direction perpendicular to the fiber axis on the nanometer scale. When X-ray incident beam was parallel to the fiber axis, a

ring pattern was appeared, which exhibited an isotropic intensity distribution based on the azimuthal scan. When combined with the results of POM and 1D WAXD, the grafted polymers PMPCS should exhibit the Φ_N phase.

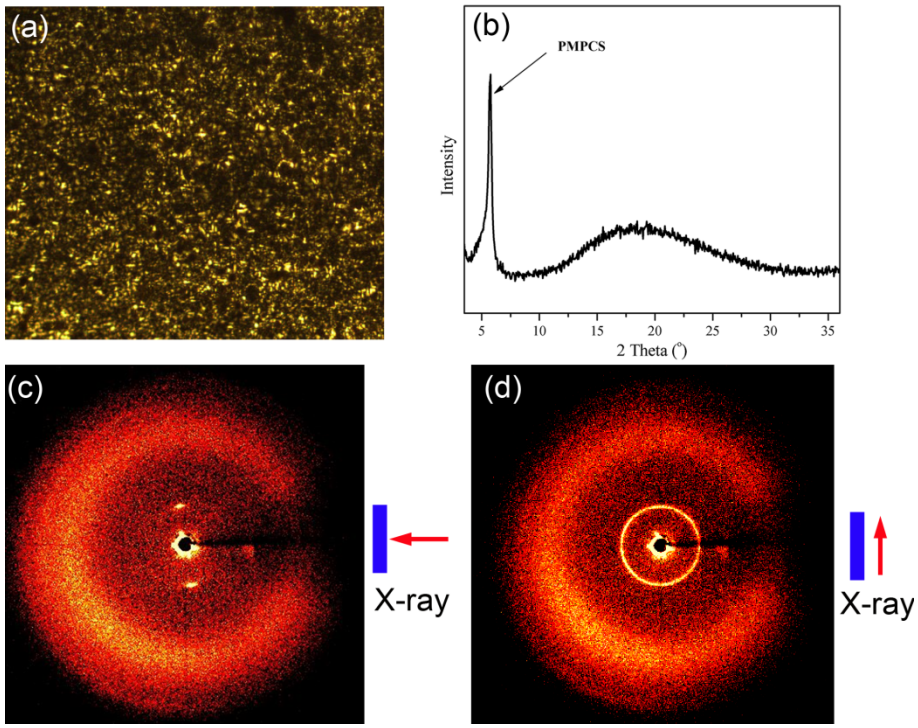

Figure 5 (a) Polarized optical microscopy (POM) images of grafted polymers PMPCS, (b) 1D WAXD patterns and (c, d) 2 D WAXD patterns of grafted polymers PMPCS.

Due to the rigid properties of the PMPCS, the length of the polymer chain can be calculated. According to the Eqn. 1 and the GPC results, the theoretical thickness of PMPCS polymer layer is 38.4 nm. In addition, the thickness can be determined from TEM images of the $BaTiO_3$@PMPCS (Figure 6), and the thickness of polymers layer is approximately 33 nm, which is slightly smaller than the theoretical value. This slightly smaller polymer thickness is due to relatively wide PDI of the measured molecular weight (Mn) of the grafted polymer PMPCS (Figure S3, Supporting

Information). The morphology of $BaTiO_3$@PMPCS is confirmed by transmission electron microscopy mapping (Figure S4, Supporting Information), and the C and O elements from PMPCS were distributed across the whole surface of the b-BT NS, which was more concentrated on the edge of b-BT NS. These results indicated that a high thickness PMPCS coating was applied to b-BT NS and the thickness of which could be controlled.

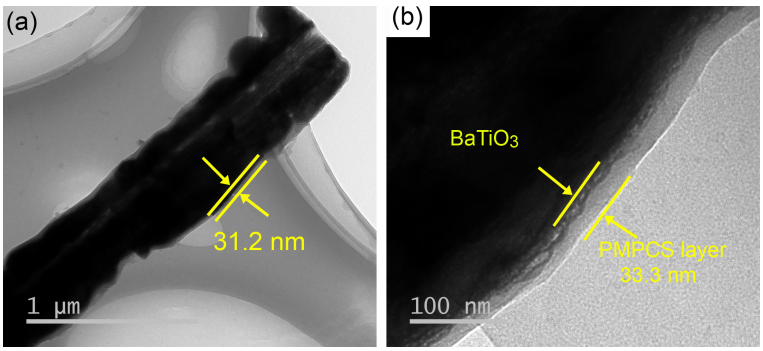

Figure 6 TEM images of b-BT NS at low (a) and high (b) magnifications.

To assess the dielectric properties of the nanocomposites formed using b-BT NS, the frequency dependent permittivity and dielectric loss of the nanocomposites with various loading levels of b-BT NS was measured over the range of 100 Hz to 10 MHz in Figure 7. It can be seen that the permittivity of the nanocomposite continuously increased on increasing the loading level of b-BT NS, which is shown in Figure 7a. For example, the permittivity of the nanocomposites at 1 kHz are 6.9, 14.3, 19.8 and 22.5 when the loading level of b-BT NS gradually increased from 0, 2.5, 5 andx 7.5 vol%. In addition, a decrease in permittivity with increasing frequency has been observed due to the existence of some electrical conductivity in the material, which has been simulated using resistor-capacitor networks.[34] Due to the dense coated layer

of PMPCS, all of the nanocomposites exhibited a low dielectric loss, especially in the low frequency range. Even when the nanocomposite incorporated with the highest b-BT NS loading of 7.5 vol%, the dielectric loss at 1 kHz was still as low as 0.05.

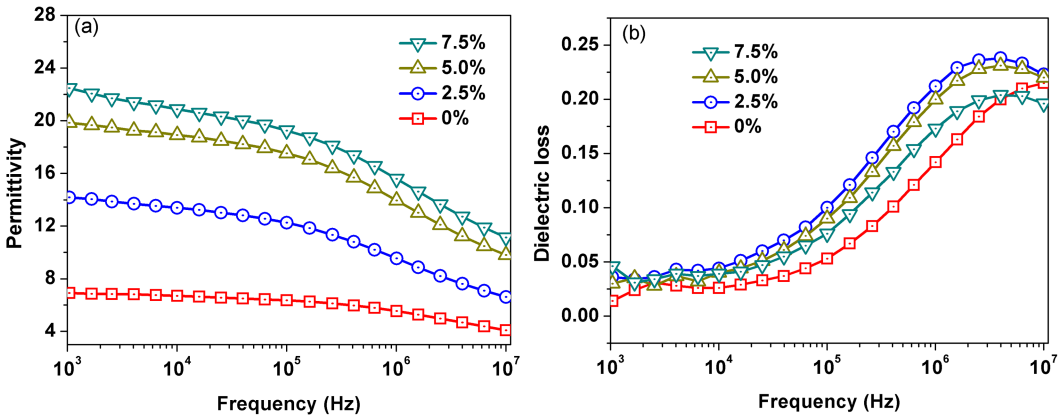

Figure 7 (a) Relative permittivity, and (b) dielectric loss of $BaTiO_3$@PMPCS/P(VDF-HFP) nanocomposites.

According to the equation $U = \int EdD$, where E is the applied electric field, D is the electric displacement, it is found that the breakdown strength is the key parameter to achieve a high discharge energy density (U) of the composite.[35, 36] The breakdown strength of the $BaTiO_3$@PMPCS/P(VDF-HFP) nanocomposites with various volume fractions of fillers is shown in Figure 8, which is analyzed with a two-parameter Weibull distribution function (Figure 8a). The equation as:

$$P(E) = 1 - \exp[-(E/E_0)^{\beta}] \qquad (2)$$

The characteristic breakdown strength (E_0) is obtained when the cumulative probability of electric failure (P(E)) equaled at 63.2%, β is the shape parameter.[37] As can be seen from Figure 8, the pure (unfilled) P(VDF-HFP) polymer exhibited the highest breakdown strength of 399.2 kV/mm, which gradually decreased with an

increase of the b-BT NS content. For, example, the sample with 2.5 vol% b-BT NS possessed a breakdown strength of 345.6 kV/mm while at 7.5 vol% the breakdown strength was 254.2 kV/mm. Inevitable defects are formed and increased with the increase of b-BT NS loadings and the internal electric field is enhanced, thus the breakdown strength continuously decrease when the b-BT NS loading level increased.

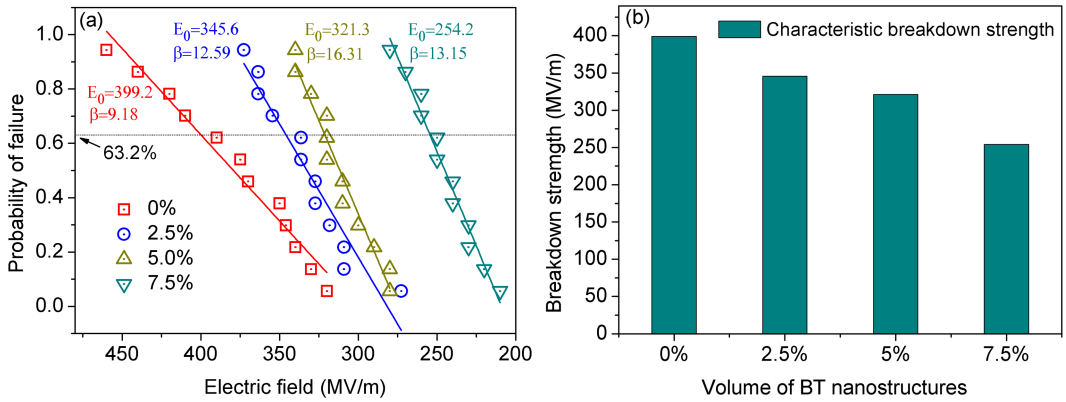

Figure 8 (a) Weibull distribution of the dielectric breakdown strength of nanocomposites filled with various $BaTiO_3$@PMPCS, (b) variation of characteristic breakdown strength from Weibull distribution for samples with various volume fractions of fillers.

The energy density of the samples can be calculated from the electric displacement−electric field ($D-E$) loops. The D-E loops of the nanocomposites with various loading levels of b-BT NS and electric field levels are shown in Figure S5 (Supporting Information). As can be seen, the electric displacement of the nanocomposites significantly increased with increased loading of $BaTiO_3$@PMPCS at the same electric field. For example, the saturated electric displacement of the nanocomposites with 2.5 and 5.0 vol% $BaTiO_3$@PMPCS at 300 MV/m are 4.37 and

7.81 μC/cm^2, the remanent electric displacement is 1.07 and 1.97 μC/cm^2. Obviously, the nanocomposites with relatively high loading levels of $BaTiO_3$@PMPCS can effectively improve the energy density. Thus, the energy density of the nanocomposite with 7.5 vol% $BaTiO_3$@PMPCS at a relatively low electric field of 240 kV/mm reached 7.1 J/cm^3, which was much larger than pure P(VDF-HFP) at the same electric field. Due to the dielectric loss and leakage current of the dielectric nanocomposites, parts of the charged energy will be converted into other energy and cannot be discharged, thus it is necessary to evaluate the energy efficiency of the nanocomposites according to the equation,

$$\eta=U_{dis}/U_{sto} \quad (3)$$

Where η, U_{dis} and U_{sto} represents the energy efficiency, discharged energy density and stored energy densities, respectively. The η calculated from the *D–E* loops of the nanocomposites with various $BaTiO_3$@PMPCS loading levels and electric fields are shown in Figure 9b. As can be seen, the pure P(VDF-HFP) sample showed the highest η, which decreased with the increase of $BaTiO_3$@PMPCS. Due to the relatively low remnant polarization, the samples obtained a high η of 55.1 % when the $BaTiO_3$@PMPCS loading was 5.0% vol at 300 MV/m, and the sample obtained a highest discharged energy density of 7.5 J/cm^3.

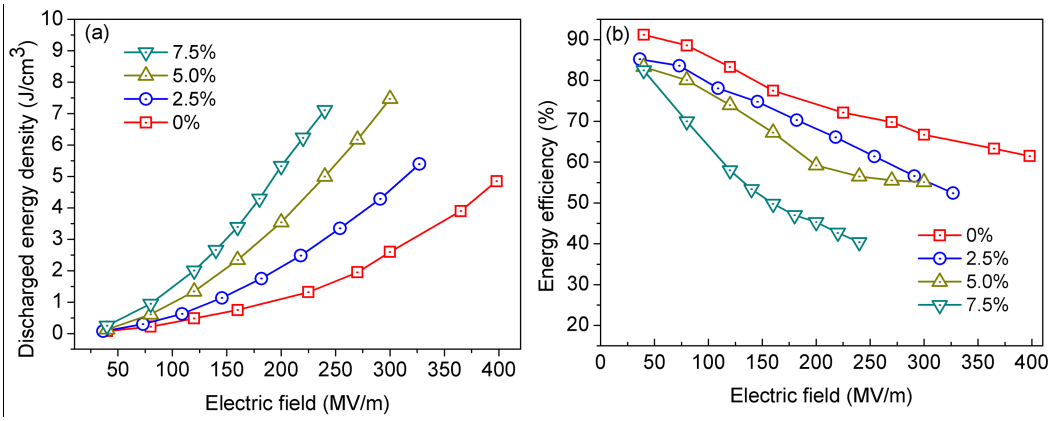

Figure 9 (a) Discharged energy densities, (b) energy efficiency of the nanocomposites with the electric field and $BaTiO_3$@PMPCS loadings.

Conclusion

$BaTiO_3$ nanowires were synthesized by a two-step hydrothermal method, which was engineered by rigid-polymers PMPCS via a surface-initiated RAFT method. The relative permittivity of the nanocomposite continuously increased with the level of $BaTiO_3$ nanowires loading increased, while also maintaining a relatively low dielectric loss (<0.05 at 1 kHz). Due to the properties of the rigid polymer, the coated layer thickness can be designed. PMPCS layer with large thickness of approximately 33 nm was coated on the surface of $BaTiO_3$ nanowires. Thus, a high discharged energy density of 7.5 J/cm^3 and an energy efficiency of 55.1% at 300 MV/m were simultaneously achieved. This work proved that utilizing a rigid liquid-crystalline polymer to engineer the surface of $BaTiO_3$ nanowires is an effective route to prepare high performance capacitors.

Supporting Information

Electronic Supplementary Information (ESI) available: [^{1}H NMR spectra of

CPDB-NHS; Digital pictures of settle ability of $BaTiO_3$, $BaTiO_3$-NH_2, $BaTiO_3$-CPDB and $BaTiO_3$-PMPCS suspension; Gel permeation chromatographic (GPC) traces of the PMPCS polymer cleaved from different core-shell structured $BaTiO_3$@PMPCS nanostructures; Mapping pattern images of $BaTiO_3$@PMPCS nanostructures; D-E loops of the nanocomposites with various $BaTiO_3$@PMPCS loadings.

References

(1) Commission, E.; Commission, E., Europe 2020: A Strategy for Smart, Sustainable and Inclusive Growth. *European Commission* **2010**.

(2) Li, Q.; Han, K.; Gadinski, M. R.; Zhang, G. Z.; Wang, Q., High Energy and Power Density Capacitors from Solution-Processed Ternary Ferroelectric Polymer Nanocomposites. *Adv. Mater.* **2014,** *26* (36), 6244-6249.

(3) Dang, Z. M.; Yuan, J. K.; Yao, S. H.; Liao, R. J. Flexible nanodielectric materials with high permittivity for power energy storage. Adv. Mater. 2013, 25, 6334-6665.

(4) Huang, X.; Jiang, P. Core-shell Structured High-k Polymer Nanocomposites for Energy Storage and Dielectric Applications. Adv. Mater. 2015, 27, 546-554.

(5) Li, Q.; Chen, L.; Gadinski, M. R.; Zhang, S.; Zhang, G.; Li, H.; Haque, A.; Chen, L. Q.; Jackson, T.; Wang, Q. Flexible High-temperature Dielectric mMaterials from Polymer Nanocomposites. Nature 2015, 523, 576-579.

(6) Zhang, X.; Shen, Y.; Zhang, Q.; Gu, L.; Hu, Y.; Du, J.; Lin, Y.; Nan, C. W., Ultrahigh Energy Density of Polymer Nanocomposites Containing $BaTiO_3$@TiO_2

Nanofibers by Atomic-Scale Interface Engineering. *Adv. Mater.* **2015,** *27* (5), 819-824.

(7) Tang, H.; Sodano, H. A., Ultra High Energy Density Nanocomposite Capacitors with Fast Discharge Using $Ba_{0.2}Sr_{0.8}TiO_3$ Nanowires. *Nano Lett.* **2013,** *13* (4), 1373-1379.

(8) Zheng, M. S.; Zha, J. W.; Yang, Y.; Han, P.; Hu, C. H.; Dang, Z. M. Enhanced Breakdown Strength of Poly(vinylidene fluoride) Utilizing Rubber Nanoparticles for Energy Storage Application. *Appl. Phys. Lett*. 2016, 109, 072902.

(9) Fredin, L. A.; Li, Z.; Ratner, M. A.; Lanagan, M. T.; Marks, T. J., Enhanced Energy Storage and Suppressed Dielectric Loss in Oxide Core-Shell-Polyolefin Nanocomposites by Moderating Internal Surface area and Increasing Shell Thickness. *Adv. Mater.* **2012,** *24* (44), 5946–5953.

(10) Li, J.; Claude, J.; Norena-Franco, L. E.; Sang, I. S.; Wang, Q., Electric Energy Storage in Ferroelectric Polymer Nanocomposites Containing Surface-Functionalized $BaTiO_3$ Nanoparticles. *Chem. Mater.* **2008,** *20* (20), 6304-6306.

(11) Luo, H.; Zhang, D.; Jiang, C.; Yuan, X.; Chen, C.; Zhou, K., Improved Dielectric Properties and Energy Storage Density of P(VDF-HFP) Nanocomposite with Hydantoin Epoxy Resin Coated $BaTiO_3$. *ACS Appl. Mater. Interfaces* **2015,** *7* (15), 8061–8069.

(12) Luo, H.; Chen, C.; Zhou, K.; Zhou, X.; Wu, Z.; Zhang, D., Enhancement of Dielectric Properties and Energy Storage Density in Poly(vinylidene

fluoride-co-hexafluoropropylene) by Relaxor Ferroelectric Ceramics. *RSC Adv.* **2015,** *5* (84), 68515-68522.

(13) Dang, Z. M.; Yuan, J. K.; Zha, J. W.; Zhou, T.; Li, S. T.; Hu, G. H. Fundamentals, Processes and Aapplications of High-permittivity Polymer–matrix Composites. Prog. Mater. Sci. 2012, 57, 660-723.

(14) Liu, S. H.; Zhai, J. W.; Wang, J. W.; Xue, S. X.; Zhang, W. Q. Enhanced Energy Storage Density in Poly(vinylidene fluoride) Nnanocomposites by a Small Loading of Suface-hydroxylated $Ba_{0.6}Sr_{0.4}TiO_3$ Nanofibers. ACS Appl. Mater. Interfaces 2014, 6, 1533-1540.

(15) Tang, H.; Zhou, Z.; Sodano, H. A., Relationship between $BaTiO_3$ Nanowire Aspect Ratio and the Dielectric Permittivity of Nanocomposites. *ACS Appl. Mater. Interfaces* **2014,** *6* (8), 5450-5455.

(16) Wang, B.; Qin, D.; Liang, G.; Gu, A.; Liu, L.; Yuan, L., High-k Materials with Low Dielectric Loss Based on Two Superposed Gradient Carbon Nanotube/Cyanate Ester Composites. *J. Phys. Chem. C* **2013,** *117* (30), 15487-15495.

(17) Pan, Z. B.; Yao, L. M.; Zhai, J. W.; Fu, D. Z.; Shen, B.; Wang, H. T.; High-Energy-Density Polymer Nanocomposites Composed of Newly-Structured One-Dimensional $BaTiO_3@Al_2O_3$ Nanofibers. *ACS Appl. Mater. Interfaces,* 2017, **DOI:** 10.1021/acsami.6b13663.

(18) Kim, P.; Doss, N. M.; Tillotson, J. P.; Hotchkiss, P. J.; Pan, M.-J.; Marder, S. R.; Li, J.; Calame, J. P.; Perry, J. W., High Energy Density Nanocomposites Based on

Surface-Modified $BaTiO_3$ and a Ferroelectric Polymer. *ACS Nano* **2009,** *3* (9), 2581-2592.

(19) Song, Y.; Shen, Y.; Liu, H.; Lin, Y.; Li, M.; Nan, C.-W., Enhanced Dielectric and Ferroelectric Properties Enduced by Dopamine-Modified $BaTiO_3$ Nanofibers in Flexible poly (vinylidene fluoride-trifluoroethylene) Nanocomposites. *J. Mater. Chem.* **2012,** *22* (16), 8063-8068.

(20) Wang, S.; Huang, X.; Wang, G.; Wang, Y.; He, J.; Jiang, P., Increasing the Energy Efficiency and Breakdown Strength of High-Energy-Density Polymer Nanocomposites by Engineering the $Ba_{0.7}Sr_{0.3}TiO_3$ Nanowire Surface via Reversible Addition–Fragmentation Chain Transfer Polymerization. *J. Phys. Chem. C* **2015**, 119 (45), 25307–25318.

(21) Dang, Z. M.; Wang, H. Y.; Xu, H. P., Influence of silane coupling agent on morphology and dielectric property in $BaTiO_3$/polyvinylidene fluoride composites. *Appl. Phys. Lett.* **2006,** *89* (11), 112902.

(22) Xie, L.; Huang, X.; Yang, K.; Li, S.; Jiang, P., "Grafting to" Route to PVDF-HFP-GMA/$BaTiO_3$ Nanocomposites with High Dielectric Constant and High Thermal Conductivity for Energy Storage and Thermal Management Applications. *J. Mater. Chem. A* **2014,** *2* (15), 5244-5251.

(23) Yang, K.; Huang, X.; Huang, Y.; Xie, L.; Jiang, P., Fluoro-Polymer@ $BaTiO_3$ Hybrid Nanoparticles Prepared via RAFT Polymerization: Toward Ferroelectric Polymer Nanocomposites with High Dielectric Constant and Low Dielectric Loss for Energy Storage Application. *Chem. Mater.* **2013,** *25* (11), 2327-2338.

(24) Caruso, F., Nanoengineering of Particle Surfaces. *Adv. Mater.* **2001,** *13* (1), 11-22.

(25) Yang, K.; Huang, X.; Zhu, M.; Xie, L.; Tanaka, T.; Jiang, P., Combining RAFT Polymerization and Thiol-ene Click Reaction for Core-shell Structured Polymer@$BaTiO_3$ Nanodielectrics with High Dielectric Constant, Low Dielectric Loss, and High Energy Storage Capability. *ACS Appl. Mater. Interfaces* **2014,** *6* (3), 1812-1822.

(26) Chen, S.; Luo, H.; Xie, H. L.; Zhang, H. L., Synthesis of Mesogen-Jacketed Liquid Crystalline Polymers with Long Symmetry Mesogenic Core Containing Two Biphenyls. *Polymer* **2013,** *54* (7), 1794-1802.

(27) Chen, X. F.; Shen, Z.; Wan, X. H.; Fan, X. H.; Chen, E. Q.; Ma, Y.; Zhou, Q. F., Mesogen-Jacketed Liquid Crystalline Polymers. *Chem. Soc. Rev.* **2010,** *39* (8), 3072-3101.

(28) Yu, Y.; Nakano, M.; Ikeda, T., Photomechanics: Directed Bending of a Polymer Film by Light. *Nature* **2003,** *425* (6954).

(29) Peng, C.; Turiv, T.; Guo, Y.; Shiyanovskii, S. V.; Wei, Q.-H.; Lavrentovich, O. D., Control of Colloidal Placement by Modulated Molecular Orientation in Nematic Cells. *Science Advances,* **2016**, 2, 1600932.

(30) Lv, J. A.; Liu, Y.; Wei, J.; Chen, E.; Qin, L.; Yu, Y., Photocontrol of Fluid Slugs in Liquid Crystal Polymer Microactuators. *Nature* **2016,** *537* (7619).

(31) Zhang, D.; Liu, Y. X.; Xinhua Wan, A.; Zhou, Q. F., Synthesis and Characterization of A New Series of "Mesogen-Jacketed Liquid Crystal Polymers"

Based on the Newly Synthesized Vinylterephthalic Acid. *Macromolecules* **1999,** *32* (16), 5183-5185.

(32) Shi, L. Y.; Zhou, Y.; Fan, X. H.; Shen, Z., Remarkably Rich Variety of Nanostructures and Order–Order Transitions in a Rod–Coil Diblock Copolymer. *Macromolecules* **2013,** *46* (46), 5308-5316.

(33) Chen, S.; Jie, C.; Xie, H.; Zhang, H., Influence of Alkoxy Tail Length on the Self-organization of Hairy-rod Polymers Based on Mesogen-Jacketed Liquid Crystalline Polymers. *J. Polym. Sci., Part A: Polym. Chem.* **2012,** *50* (19), 3923-3935.

(34) Wang, G.; Huang, X.; Jiang, P., Tailoring Dielectric Properties and Energy Density of Ferroelectric Polymer Nanocomposites by High-k Nanowires. *ACS Appl. Mater. Interfaces* **2015,** *7* (32), 18017–18027.

(35) Hao, X.; Zhai, J.; Yao, X., Improved Energy Storage Performance and Fatigue Endurance of Sr^{-} Doped $PbZrO_3$ Antiferroelectric Thin Films. *J. Am. Ceram. Soc.* **2009,** *92* (5), 1133-1135.

(36) Rabuffi, M.; Picci, G., Status Quo and Future Prospects for Metallized Polypropylene Energy Storage Capacitors. *IEEE Transactions on Plasma Science* **2002,** *30* (5), 1939-1942.

(37) Hu, P.; Shen, Y.; Guan, Y.; Zhang, X.; Lin, Y.; Zhang, Q.; Nan, C. W., Topological-Structure Modulated Polymer Nanocomposites Exhibiting Highly Enhanced Dielectric Strength and Energy Density. *Adv. Funct. Mater.* **2014,** *24* (21), 3172–3178.